Article

ExTzBox: A Glowing Cyclophane for Live-Cell Imaging

Indranil Roy, Sharan Bobbala, Jiawang Zhou, Minh T. Nguyen, Siva Krishna Mohan Nalluri, Yilei Wu, Daniel Ferris, Evan Alexander Scott, Michael R. Wasielewski, and J. Fraser Stoddart

J. Am. Chem. Soc., **Just Accepted Manuscript** • DOI: 10.1021/jacs.8b03066 • Publication Date (Web): 17 May 2018

JACS
JOURNAL OF THE AMERICAN CHEMICAL SOCIETY

ExTzBox: A Glowing Cyclophane for Live-Cell Imaging

Indranil Roy,[†] Sharan Bobbala,[‡] Jiawang Zhou,[†] Minh T. Nguyen,[†] Siva Krishna Mohan Nalluri,[†] Yilei Wu,[†] Daniel P. Ferris,[†] Evan Alexander Scott,[‡] Michael R. Wasielewski[†,∥] and J. Fraser Stoddart[*,†,§]

[†]*Department of Chemistry,* [‡]*Department of Biomedical Engineering,* [∥]*Argonne–Northwestern Solar Energy Research (ANSER) Center, Northwestern University, 2145 Sheridan Road, Evanston, Illinois 60208-3113, USA*
[§]*Institute of Molecular Design and Synthesis, Tianjin University, 92 Weijin Road, Nankai District, Tianjin, 300072, P. R. China*

*E-mail: stoddart@northwestern.edu

MAIN TEXT

***Correspondence Address**

Professor J. Fraser Stoddart
Department of Chemistry
Northwestern University
2145 Sheridan Road
Evanston, IL 60208 (USA)
Email: *stoddart@northwestern.edu*

■ ABSTRACT

The ideal fluorescent probe for live-cell imaging is bright, non-cytotoxic and can be delivered easily into the living cells in an efficient manner. The design of synthetic fluorophores, having all three of these properties, however, has proved to be challenging. Here, we introduce a simple, yet effective, strategy based on well-established chemistry for designing a new class of fluorescent probes for live-cell imaging. A box-like hybrid cyclophane, namely **ExTzBox**•4X (**6**•4X, X = PF_6^-, Cl^-), has been synthesized by connecting an extended viologen (ExBIPY) and a dipyridyl thiazolothiazole (TzBIPY) unit in an end-to-end fashion with two *p*-xylylene (*p*-Xy) linkers. Photophysical studies show that **6**•4Cl has a quantum yield, Φ_F = 1.00. Furthermore, unlike its $ExBIPY^{2+}$ and $TzBIPY^{2+}$ building units, **6**•4Cl is non-cytotoxic to RAW 264.7 macrophages, even with a loading concentration as high as 100 μM, presumably on account of its rigid box-like structure which prevents its intercalation into DNA and inhibits any other interactions with it. After gaining an understanding of the toxicity profile of **6**•4Cl, we employed it in live-cell imaging. Confocal microscopy has demonstrated that $\mathbf{6}^{4+}$ is taken up by the RAW 264.7 macrophages, allowing the cells to glow brightly with blue laser excitation, without any hint of photobleaching or disruption of normal cell behavior under the imaging conditions. By contrast, the acyclic reference compound **Me_2TzBIPY**•2Cl (**4**•2Cl) shows very little fluorescence, inside the cells, which is quenched completely under the same imaging conditions. The in vitro cell investigations underscore the significance of using highly fluorescent box-like rigid cyclophanes for live-cell imaging.

INTRODUCTION

Live-cell imaging using fluorescent probes[1] has become an indispensable tool for medical diagnostics as well as for biological studies, particularly when investigating real-time endocytic pathways[2]. This information, which allows us to follow the movement of intracellular proteins in living cells with extraordinary detail[3], is an essential tool for understanding how biological systems function. These fluorescent probes provide high sensitivity and great versatility, while perturbing minimally the cells under investigation. Today, an expanded selection of probes, including organic dyes[4], metal-ligand complexes[5], polymer nanostructures[6] and nanoparticles[7] are available for use. Small molecules are currently being used, for the most part to image live cells.[8] Special attention is still required, however, in order to overcome, the common and the most important imaging-related issues, such as water solubility,[9] pH sensitivity,[10] photostability,[11] membrane permeability,[12] aggregation-induced quenching,[13] and cell viability.[14] Since the design and synthesis of new fluorophores, having all of these properties, has proved[15] to be challenging, continuous effort and experimentation are required.

The fundamental principles of bioimaging need to be considered carefully during the development of a new probe. An ideal fluorescent imaging probe must meet the following stringent requirements: it must be (i) deliverable easily and efficiently into living cells, (ii) photostable and bright in biological settings in order to minimize background noise and maximize spatial resolution, (iii) non-cytotoxic and non-interfering with endogenous and cellular processes, and (iv) capable of sustaining a balance between hydrophilicity and hydrophobicity in the context of water solubility, membrane permeability, and cellular retention. It is well known that the tuning of the photophysical properties and functionalities of a fluorophore can be altered by chemical means. Numerous examples in literature show that chemical modifications can

indeed increase fluorescence quantum yields,[16] brightness,[17] photostability,[18] and cell permeability[12] of fluorescent molecules. Further developments in the chemistry of small-molecule imaging probes will aid and abet the discovery of additional structural features that will have a large impact on fluorophore brightness, photostability, pH stability and cytotoxicity, particularly if they are placed in an enclosed environment.

A box-like, rigid cyclophane − namely, **Blue Box** − was synthesized by us[19] almost three decades ago. Since then, many variants[20] have been prepared and utilized in host-guest chemistry,[21] as well as in the production of mechanically interlocked molecules,[22] and gels, not to mention applications such as polyaromatic hydrocarbon (PAH) extractions,[23] catalyses,[24] electron transfers,[25] molecular electronics,[26] and molecular machines.[27] We anticipated that these box-like, rigid cyclophanes, which have remained unexplored in the field of bioimaging, might have considerable potential provided they are fluorescent. Synthetically, these cyclophanes are easy to prepare and their properties can be modified by changing their building units or introducing different functional groups into the cyclophanes by means of covalent bonds.[28] In addition, they can accommodate a library of guest molecules in their cavities, thus forming host-guest inclusion complexes.[21] The combination of structural modifications, along with host-guest chemistry,[21] could open the door for the development of the next generation imaging probes.[29] We have also envisioned that −unlike some small fluorescent molecules or polycyclic aromatic dyes[30] − these tetracationic box-like cyclophanes may be less likely to intercalate into or interact electrostatically with DNA on account of their bulky structures, and hence may have low cytotoxicity. In order to understand their potential as imaging agents, it is necessary to (i) establish their toxicity profiles, (ii) demonstrate their cellular uptake and (iii) delineate the cells at least in vitro. We anticipated that, rather than incorporating a fluorescent guest inside the

cavity of a rigid, box-like cyclophane, an insertion of a small fluorophore in between one of the two bipyridinium units in the **Blue box**, might produce a fluorescent host that could be used for live-cell imaging, while reserving the option of accommodating a guest[21] with some additional functions. The unique box-like, cyclic structures, which could also be considered as small molecule analogues to fluorescent proteins, may shield their fluorophore part from the outside environment by enclosing aromatic system and may address several issues that fluorescence proteins possess, such as pH stability and photostability. We selected thiazolothiazole[16,31] as the fluorophore since it possesses excellent photophysical properties such as strong fluorescent emission, high fluorescent quantum yield[31] and is easy to incorporate synthetically between the bipyridinium units of one side of the **Blue Box**. In order to match its length, we opted for an extended bipyridinium unit on the other side of the cyclophane.

Here, we report the rational design and synthesis of a rigid, box-like hybrid cyclophane, **ExTzBox**•4X (**6**•4X, X = PF_6^-, Cl^-), containing one ExBIPY (**1**)unit and one TzBIPY (**3**) unit, which are bridged together by two *para*-xylylene (*p* − Xy) linkers. This constitutionally asymmetric tetracationic cyclophane is readily soluble in both polar organic solvents, e.g., MeCN, Me_2CO, and DMF as its PF_6^- salt, and in H_2O as either its Cl^- or TFA^- salt. Combined steady-state and time-resolved experiments were carried out in order to investigate the photophysical processes of **6**•4Cl. 3-(4,5-Dimethylthiazol-2-yl)-2,5-diphenyltetrazolium bromide (MTT) assays were performed so as to understand toxicity profiles of **6**•4Cl and its building units in the reference salts, **Me_2ExBIPY**•2Cl (**2**•2Cl) and **Me_2TzBIPY**•2Cl (**4**•2Cl). Finally, **6**•4Cl was employed for live-cell imaging. Our investigations demonstrate that $\mathbf{6}^{4+}$ enters the lysosomes of living macrophages, allowing the cells to glow brightly under irradiation of blue laser light.

■ RESULTS AND DISCUSSION

The hybrid cyclophane, **ExTzBox**•4X (**6**•4X, X = PF_6^-, Cl^-) was synthesized (Scheme 1) without the use of a template. In a typical experiment, the reaction of 2,5-di(pyridin-4-yl)thiazolo[5,4-d]thiazole (**TzBIPY, 3**) and **DB**•2PF_6 (**5**•2PF_6) in 1:1 ratio in dry MeCN and in the presence of ~5 mol% $^nBu_4NI$ under refluxing conditions was followed by the addition of solid $^nBu_4NCl$ to precipitate the crude product, which was washed with CH_2Cl_2 and dissolved in H_2O. Counterion exchange (NH_4PF_6) produced a precipitate, which was filtered and subjected to reverse-phase column chromatography, affording **6**•4PF_6 in 25 % yield based on **5**•2PF_6. See Supporting Information. A combination of ^1H and ^{13}C nuclear magnetic resonance (NMR) spectroscopy and high-resolution mass spectrometry (HRMS) confirmed (Figure S1-3) the formation of **6**•4PF_6. Water soluble **6**•4Cl was obtained from **6**•4PF_6, following counterion exchange ($^nBu_4NCl$ / MeCN). See Supporting Information for the detailed synthetic procedures and spectroscopic analyses for each compound.

Further evidence for cyclophane formation comes from single-crystal X-ray diffraction (XRD) analysis. Single crystals were grown by vapor diffusion of *i*-Pr_2O into a MeCN solution of **6**•4PF_6 for 3−4 days. The solid-state (super)structure reveals (Figure 1) a box-like cyclophane for $\mathbf{6}^{4+}$ measuring 15.6 Å in length, and 6.6 and 7.1 Å in width at its periphery and center, respectively. The two torional angles between the pyridinium and phenylene rings associated with the $ExBIPY^{2+}$ unit are 19° and 38°. The two torsional angles between the pyridinium and thiazolothiazole rings, however, at the $TzBIPY^{2+}$ unit are 4° and 23°. This flatter conformation for the $TzBIPY^{2+}$ unit in $\mathbf{6}^{4+}$ is presumably a result of the absence of H atoms on the thiazolothiazole unit and its planar fused-ring geometry. The extended solid-state superstructure of $\mathbf{6}^{4+}$ reveals that $ExBIPY^{2+}$ and $TzBIPY^{2+}$ units are facing each other with a short intermolecular π···π distance of 3.31 Å from the centroid of $TzBIPY^{2+}$ to the phenylene ring in

ExBIPY^{2+}. C-H···π Interactions are observed between the *p*-Xy rings and the adjacent cyclophanes (C-H···π distance of 2.7 Å). The overall superstructure of **6**$^{4+}$ reveals (Figure 1e) a zigzag arrangement of the cyclophanes.

The steady-state absorption and emission spectra of **6**•4Cl in H_2O are shown in Figure 2a. The absorption spectrum of **6**•4Cl exhibits absorbance maxima in its UV region at λ_{max}= 320 nm and in its visible region at λ_{max}= 410 nm, both bands being characteristic of ExBIPY^{2+} and TzBIPY^{2+} units, respectively. The absorption spectrum of the reference **Me$_2$TzBIPY^{2+} (4^{2+})**, is similar to that of **6**$^{4+}$ except that it has a lower molar extinction coefficient and a slightly blue-shifted absorption maximum, suggesting (Figure S5) that, photophysically, the thiazolothiazole unit in **6**$^{4+}$ behaves as a reference monomer. The cyclophane **6**$^{4+}$ shows bright blue fluorescence in H_2O and possesses an emission maximum at λ_{max} = 470 nm with a fluorescence quantum yield of unity. The cyclophane **6**$^{4+}$ is photostable and retains its photophysical properties in H_2O for several months under natural daylight. In order to assess the photostability of **6**$^{4+}$, photobleaching studies were performed under UV flashlight (18 W, 395 nm) and the results were compared with a commercially available nucleic acid staining dye, hoechst 33258. The experimental results (Figure S6) show a little loss of absorbance intensity of **6**$^{4+}$ after 60 min of UV light irradiation, an observation which is comparable to the photostability of hoechst dye. The cyclophane **6**$^{4+}$ also endures strong acidic conditions (pH = 1) and operates in a broad pH range (pH = 1 to 7) without any change (Figure S7) of its fluorescence characteristics. Furthermore, the fluorescence spectrum of **6**$^{4+}$ in serum is similar to the spectrum obtained in water with slightly lower fluorescence intensity (Figure S8), indicating little influence of serum proteins on the fluorescence emission of **6**$^{4+}$.

In order to investigate the excited-state properties of $\mathbf{6}^{4+}$, especially in relation to its fluorescence quantum yield of unity, we applied femtosecond and nanosecond transient absorption −fsTA and nsTA, respectively − to **6**•4Cl as the target compound and **4**•2Cl as the reference. Upon photoexcitation at 414 nm, **4**•2Cl shows two positive features at ca. 500 and above 800 nm, which can be assigned (Figure S9a) to the excited-state absorption (ESA) of the reference compound. Meanwhile, two negative bands centered on 390 and 445 nm can be ascribed to ground-state bleaching and stimulated emission, respectively. Global analysis reveals that the nascent singlet excited state undergoes (Figure S9c) two sequential structural relaxations with timescales of 0.95 and 134 ps, before decaying back to S_0. The singlet lifetime is estimated to be 2.14 ns, a value which is consistent with the nsTA (2.1 ns, Figure S10) and time-resolved fluorescence results (2.04 ns, Figure S5). In the case of the target compound **6**•4Cl, very similar photo-induced dynamics can be observed (Figure 2b). The transient features in **6**•4Cl strongly resemble those in **4**•2Cl, with close structural relaxation timescales (1.18 and 211 ps), as well as a singlet lifetime (2.45 ns, Figure S11), all of which agree well with the nsTA (2.5 ns, Figure S12) and the time-resolved fluorescence (2.15 ns, Figure 2a) measurements. The similarities in spectrometric behavior between $\mathbf{6}^{4+}$ and $\mathbf{4}^{2+}$ indicate unambiguously that no electron transfer occurs within **6**•4Cl when excited at 414 nm. Since there are no additional non-emissive relaxation pathways evident for $\mathbf{6}^{4+}$, it makes sense that the fluorescence quantum yield of $\mathbf{6}^{4+}$ in H_2O is unity, a value which is slightly higher (Figure S5) than that (Φ_F = 0.95) of $\mathbf{4}^{2+}$. The observed increase in fluorescence efficiency in $\mathbf{6}^{4+}$, relative to that in $\mathbf{4}^{2+}$, can also be attributed to the additional rigidity imposed by the cyclophane structure which reduces certain vibrational degrees of freedom responsible for the radiationless internal conversion process.

For a better understanding of the electronic and fluorescence properties of $\mathbf{6}^{4+}$, DFT and TDDFT calculations were carried out at the cam-B3LYP/6-31G** level of theory. The lowest absorption band in $\mathbf{6}^{4+}$ is predicted to be the HOMO-LUMO transition, and the electron in both the HOMO and LUMO of $\mathbf{6}^{4+}$ is located (Figure S13) only in the $TzBIPY^{2+}$ component. This observation supports the transient absorption interpretation, i.e. no charge transfer happens from the *p*-Xy components to the $TzBIPY^{2+}$ or the $ExBIPY^{2+}$ when $\mathbf{6}^{4+}$ is excited at the lowest absorption band.[32]

Analysis (Figure 2c) of the cyclic voltammogram (CV) of hybrid **6**•$4PF_6$, reference **4**•$2PF_6$ and their comparison with those of the predecessors **ExBox**•$4PF_6$ and **2**•$2PF_6$ provides useful insight into the electrochemical behavior of the hybrid cyclophane which is comprised of two different redox-active units.[23] The CV of **4**•$2PF_6$ consists of two reversible two-electron redox couples at −0.43 and −0.57 V, where the potentials of the two cathodic peaks are separated by 140 mV, suggesting that the thiazolo[5,4-d]thiazole unit provides a good electronic communication between the two pyridinium rings (Figure S16). On the contrary, the CV of **2**•$2PF_6$ consists essentially of one broad redox couple where the two one-electron reduction waves overlap completely at −0.82 V, an observation which indicates that the two bipyridinium redox centers are not communicating and behave quite independently of one another.[23] The hybrid **6**•$4PF_6$, however, consists of four well-separated reversible one-electron redox couples at −0.35, −0.47, −0.75 and −0.85 V, originating from the $TzBIPY^{2+}$ and $ExBIPY^{2+}$ units. The peaks at −0.35 and −0.47 V can be assigned to two one-electron reductions of the $TzBIPY^{2+}$ unit while the peaks at −0.75 and −0.85 V can be assigned to two one-electron reductions of the $ExBIPY^{2+}$ unit. The separation between cathodic and anodic peaks reveals that heterogeneous electron transfer is fast on the timescale of the experiment employing a scan rate of 100 mVs^{-1}. This

observation reflects the level of electronic communication among the redox centers of $TzBIPY^{2+}$ and $ExBIPY^{2+}$, as well as in between the pyridinium units present within $TzBIPY^{2+}$ and $ExBIPY^{2+}$. This cycle can be repeated multiple times, a situation which suggests (Figure S14) that **6**•$4PF_6$ is electrochemically stable. The formation of the first two redox species — namely, $\mathbf{6}^{\bullet(3+)}$ and $\mathbf{6}^{2+}$ — centered primarily on the Tz ring of the $TzBIPY^{2+}$ unit, whereas the third and fourth one-electron reductions occur on the $ExBIPY^{2+}$ unit, leading to the formation of $\mathbf{6}^{(3\bullet)+}$ and the fully reduced species, is shifted to lower potentials and is therefore more difficult to reduce. The redox potentials determined from CV match (Figure S14) those measured from differential pulse voltammetry (DPV). Figure S15 shows the impact of varying scan rates on the voltammetric current response and peak potential at the **6**•$4PF_6$. The current values increase with an increase in the scan rate, while the peak to peak potentials almost remain unchanged, which is indicative of a reversible redox system.

The bright and highly fluorescent nature of $\mathbf{6}^{4+}$ with a quantum yield reaching unity could potentially make it a good candidate for live-cell imaging. It has to be non-cytotoxic, however, to cells or, in other words, cells should be viable in the presence of $\mathbf{6}^{4+}$. Polycyclic aromatic compounds are known[30,33] to intercalate into the DNA and some small molecules containing amines, amides, aromatic rings, pyridines tend to bind double-stranded DNA by virtue of different means including electrostatic attractions, and intercalation between base pairs.[34] Theses interactions hinder the function of various enzymes and thereby induce toxicity to the living cells. We anticipated that, in comparison to the small cationic reference molecules, the rigid box-like structure of $\mathbf{6}^{4+}$ is less likely to intercalate into the DNA and may therefore possess less toxicity. We decided to investigate the in vitro toxicity of **6**•4Cl using an MTT (3-(4,5-dimethylthiazol-2-yl)-2,5-diphenyltetrazolium bromide) assay. After a 24 h incubation of RAW

264.7 cells with different concentrations of **6**•4Cl and the references **4**•2Cl and **2**•2Cl, the MTT assays were performed. The experimental results suggest that **6**•4Cl is less cytotoxic when compared with **4**•2Cl and **2**•2Cl. At a 100 μM loading concentration with **6**•4Cl, the cell viability is ~93% (Figure 3), whereas, for the references **4**•2Cl and **2**•2Cl, the viabilities were reduced to ~75% and 68%, presumably because the box-like rigid structure prevents $\mathbf{6}^{4+}$ from intercalating into the DNA unlike the reference compounds. We observed a similar trend for other rigid cyclophanes **BlueBox** and **ExBox** as well (Figure S17). For example, at 100 μM loading concentration of **BlueBox**, the viability of the RAW 264.7 cells is over 96%, however in the case of the reference dimethyl viologen, popularly known as paraquat, only ~63% of cells remain viable, an observation which matches with paraquat toxicity reported elsewhere in literature.[35] The cell viability of **6**•4Cl obtained from MTT assay was further confirmed by a fluorescence-based Calcein AM cell viability assay (Figure S18a) as the presence of chromophores may influence MTT assay results. Furthermore, no phototoxicity of **6**•4Cl was observed when RAW 264.7 cells were incubated with different concentrations of **6**•4Cl and were irradiated with light (410 nm, 25 mW) for 15 min (Figure S18b). It is indeed an important observation for understanding the cytotoxicity of this important class of cyclophanes and exploring their biological applications.

Based on the MTT results, a 20 − 50 μM concentration range of **6**•4Cl was used for all the imaging experiments. In order to understand the ability of $\mathbf{6}^{4}$ to be internalized by cells, RAW 264.7 cells were incubated with **6**•4Cl (20 μM in PBS solution) for 4 h, followed by imaging with a confocal microscope. The acquired images showed brilliant blue emission in the cytoplasm of the cells, without altering their morphologies. For a better understanding of the internalization, **6**•4Cl was incubated with the cells in presence of a red fluorescent nuclei acid

stain, SYTO 61, which exhibits bright, red fluorescence upon binding to nucleic acids. The blue fluorescence signal of **6**•4Cl was localized predominantly predominantly in punctae at the perinuclear region of the cells (Figure 4a-d), whereas red fluorescence of SYTO 61 was observed from the nuclei. This observation suggests that there is no migration of **6**•4Cl into the nucleus. Incubation of different concentrated solutions (50−0.1 μM) of **6**•4Cl with the cells also showed bright blue fluorescence, an observation which demonstrates that different concentrations of **6**•4Cl could be used (Figure S19-20) for cell imaging, and any concentration around 0.5 μM or above is detectable in the RAW 264.7 cells and would be suitable for staining and uptake studies. This successful membrane penetration could be attributed to the tetracationic nature of the $\mathbf{6}^{4+}$.

In order to gain further evidence of cellular localization in detail, **6**•4Cl was incubated with cells in the presence of a lysosomal marker, Lyso Tracker green. Confocal microscopy images showed (Figure 4e-h) significant co-compartmentalization of the green (Lyso Tracker green) and blue (**6**•4Cl) channel emission coming from the lysosomes. A zoomed-in section (Figure 4h) shows the presence of $\mathbf{6}^{4+}$ in the lysosome, alongside Lyso Tracker green. In the control experiment, only a little fluorescence (Figure S21) was detected with the reference compound **4**•2Cl upon cell incubation. In fact, when considering the fluorescent intensity, $\mathbf{6}^{4+}$ was found six times higher than $\mathbf{4}^{2+}$ inside the RAW 264.7 cells (Figure S22). Furthermore, the fluorescence inside the cells of the reference **4**•2Cl was quenched within 3 s of laser irradiation (Figure S23) and lost its imaging capability. This observation implies the importance of box-like rigid structures in preventing photobleaching under live-cell imaging conditions.

■ CONCLUSIONS

We have demonstrated a facile synthesis and complete characterization of a rationally designed hybrid cyclophane, $\mathbf{6}^{4+}$, in a template free manner. Cyclophane **6**•4Cl is highly water-

soluble and possesses bright blue fluorescence with a quantum yield of unity when excited at the lowest absorption band, an observation which can be ascribed to no electron transfer from the *p*-Xy components to the $TzBIPY^{2+}$ or the $ExBIPY^{2+}$ unit, as revealed by time-resolved spectroscopic measurements. The **6**•4Cl is photostable in H_2O, endures strong acidic conditions, and operates in a broad pH range without any change of its fluorescence characteristics. MTT assay shows a greater than 90% cell viability after 24 h incubation with **6**•4Cl at a loading concentration as high as 100 μM. Taken all together, the potentials of the rigid cyclophane $\mathbf{6}^{4+}$ for live-cell imaging could be easily understood. Confocal microscopy images reveal that $\mathbf{6}^{4+}$ is efficiently taken up by the RAW 264.7 cells into their lysosomal compartments and exhibits bright blue fluorescence without any hint of photobleaching. A concentration-dependent study shows that around 0.5 μM or above concentration of $\mathbf{6}^{4+}$ is detectable in the RAW 264.7 cells and would be suitable for staining and uptake studies for this particular cell line. Furthermore, the fluorescence of $\mathbf{6}^{4+}$ is six times brighter inside the cells than that of the reference $\mathbf{4}^{2+}$ whose fluorescence is completely quenched within 3 s under imaging conditions. Our findings may assist the understanding of the fundamental principles for designing this new class of imaging probes by recognizing the underlying competitive photophysical processes in the context of hybrid and rigid molecular geometries. Here, we note that **6**•4Cl is first of its kind to be utilized for live cell imaging and has good potential in the field of imaging. Several challenges, however, must still be addressed, such as improving the absorbance window for better penetration, and active targeting, which is necessary for in-depth in vivo imaging. We believe that the proper choice of building units and fine-tuning of the fluorophore structure within the cyclophane structures may address these challenges. In a broader perspective, the in vitro cell studies strongly support the importance of using box-like rigid cyclophanes for live-cell imaging and

could well be the stepping stone for developing a new class of imaging probes for multiple modalities in addition to fluorescence imaging. It is also worth mentioning that the cavity of $\mathbf{6}^{4+}$ may be utilized to incorporate different guest molecules, with various imaging modalities such as photoacoustic, ultrasound, PET or MRI, leading to the development of supramolecular multimodal-imaging platforms. Guest molecules having therapeutic properties could also be incorporated inside the cyclophane cavity, which holds promise for the development of supramolecular theranostic agents.

■ ASSOCIATED CONTENT

Supporting Information

Experimental details, including synthesis, NMR and supportive figures. This material is available free of charge via the Internet at http://pubs.acs.org.

■ AUTHOR INFORMATION

Corresponding Author

*stoddart@northwestern.edu

Notes

The authors declare no competing financial interest.

■ ACKNOWLEDGEMENTS

This research is part of the Joint Center of Excellence in Integrated Nano-Systems (JCIN) at King Abdulaziz City of Science and Technology (KACST) and Northwestern University (NU). The authors would like to thank both KACST and NU for their continued support of this research. This work was also supported by the Chemical Sciences, Geosciences, and Biosciences Division, Office of Basic Energy Sciences, DOE under grant no. DE-FG02-99ER14999 (M.R.W.). Y.W. thanks the Fulbright Scholar Program for a Fellowship and the NU International Institute of Nanotechnology for a Ryan Fellowship.

■ REFERENCES

(1) (a) Fernández-Suárez, M.; Ting, A. Y. *Nat. Rev. Mol. Cell Biol.* **2008**, *9*, 929–943. (b) Zhang, J.; Campbell, R. E.; Ting, A. Y.; Tsien, R. Y. *Nat. Rev. Mol. Cell Biol.* **2002**, *3*, 906–918.

(2) (a) Grossi, M.; Morgunova, M.; Cheung, S.; Scholz, D.; Conroy, E.; Terrile, M.;

Panarella, A.; Simpson, J. C.; Gallagher, W. M.; O'Shea, D. F. *Nat. Commun.* **2016**, *7*, 10855. (b) Progatzky, F.; Dallman, M. J.; Lo Celso, C. *Interface Focus* **2013**, *3*, 20130001.

(3) (a) Chen, X.; Bi, Y.; Wang, T.; Li, P.; Yan, X.; Hou, S.; Bammert, C. E.; Ju, J.; Gibson, K. M.; Pavan, W. J.; Bi, L. *Sci. Rep.* **2015**, *5*, 9004. (b) Liu, Z.; Lavis, L. D.; Betzig, E. *Mol. Cell* **2015**, *58*, 644. (c) Yapici, N. B.; Bi, Y.; Li, P.; Chen, X.; Yan, X.; Mandalapu, S. R.; Faucett, M.; Jockusch, S.; Ju, J.; Gibson, K. M.; Pavan, W. J.; Bi, L. *Sci. Rep.* **2015**, *5*, 8576. (d) Doupé, D. P.; Perrimon, N. *Sci. Signal.* **2014**, *7*, re1. (e) Lukinavičius, G.; Umezawa, K.; Olivier, N.; Honigmann, A.; Yang, G.; Plass, T.; Mueller, V.; Reymond, L.; Corrêa Jr, I. R.; Luo, Z.-G.; Schultz, C.; Lemke, E. A.; Heppenstall, P.; Eggeling, C.; Manley, S.; Johnsson, K. *Nat. Chem.* **2013**, *5*, 132–139.

(4) (a) Signore, G.; Nifosì, R.; Albertazzi, L.; Storti, B.; Bizzarri, R. *J. Am. Chem. Soc.* **2010**, *132*, 1276–1288. (b) Gao, F. P.; Lin, Y. X.; Li, L. L.; Liu, Y.; Mayerhöffer, U.; Spenst, P.; Su, J. G.; Li, J. Y.; Würthner, F.; Wang, H. *Biomaterials* **2014**, *35*, 1004–1014.

(5) Roy, B.; Ghosh, A. K.; Srivastava, S.; D'Silva, P.; Mukherjee, P. S. *J. Am. Chem. Soc.* **2015**, *137*, 11916–11919.

(6) Roy, I.; Shetty, D.; Hota, R.; Baek, K.; Kim, J.; Kim, C.; Kappert, S.; Kim, K. *Angew. Chem. Int. Ed.* **2015**, *54*, 15152–15155.

(7) Wolfbeis, O. S. *Chem. Soc. Rev.* **2015**, *44*, 4743–4768.

(8) (a) Kocaoglu, O.; Carlson, E. E. *Nat. Chem. Biol.* **2016**, *12*, 472–478. (b) Long, L.; Huang, M.; Wang, N.; Wu, Y.; Wang, K.; Gong, A.; Zhang, Z.; Sessler, J. L. *J. Am. Chem. Soc*. **2018**, *140*, 1870−1875. (c) Kaloyanova, S.; Zagranyarski, Y.; Ritz, S.; Hanulova, M.; Koynov, K.; Vonderheit, A.; Müllen, K.; Peneva, K. *J. Am. Chem. Soc.* **2016**, *138*, 2881−2884.

(9) Larson, D. R., Zipfel, W. R., Williams, R. M., Clark, S. W., Bruchez, M. P., Wise, F. W., Webb, W. W. *Science* **2003**, *300*, 1434−1436.

(10) Martineau, M., Somasundaram, A., Grimm, J. B., Gruber, T. D., Choquet, D., Taraska, J. W., Lavis, L. D., Perrais, D. *Nat. Commun.* **2017**, 8, 1412.

(11) Zheng, Q.; Lavis, L. D. *Curr. Opin. Chem. Biol.* **2017**, *39*, 32–38

(12) (a) Jensen, E. C. **2012**, *295*, 2031– 2036. (b) Jing, C.; Cornish, V. W. *Acc. Chem. Res.* **2011**, *44*, 784–792. (c) Cunningham, C. W. *Mol. Pharm.* **2011**, *7*, 1301–1310.

(13) Guo, B.; Cai, X. L.; Xu, S. D.; Fateminia, S. M. A.; Liu, J.; Liang, J.; Feng, G. X.; Wu, W. B.; Liu, B. *J. Mater. Chem. B* **2016**, *4*, 4690– 4695.

(14) Hou, X.; Ke, C.; Bruns, C. J.; McGonigal, P. R.; Pettman, R. B.; Stoddart, J. F. *Nat. Commun.* **2015**, *6*, 6884.

(15) Van der Velde, J. H.; Oelerich, .; Huang, J.; Smit, J. H.; Jazi, A. A.; Galiani, S.; Kolmakov, K.; Gouridis, G.; Eggeling, C.; Herrmann, A.; Roelfes, G.; Cordes, T. *Nat.*

Commun. **2016***, 7,* 10144.

(16) (a) Johnson, J. R.; Ketcham, R. *J. Am. Chem. Soc.* **1960**, *82*, 2719–2724. (b) Woodward, A. N.; Kolesar, J. M.; Hall, S. R.; Saleh, N. A.; Jones, D. S.; Walter, M. G. *J. Am. Chem. Soc.* **2017**, *139*, 8467–8473.

(17) Zheng, Q.; Juette, M. F.; Jockusch, S.; Wasserman, M. R.; Zhou, Z.; Altman, R. B.; Blanchard, S. C. *Chem. Soc. Rev.* **2014**, *43*, 1044–1056.

(18) Hyun, H.; Owens, E. A.; Narayana, L.; Wada, H.; Gravier, J.; Bao, K.; Frangioni, J. V.; Choi, H. S.; Henary, M. *RSC Adv.* **2014**, *102*, 58762–58768.

(19) Asakawa, M.; Dehaen, W.; L'abbé, G.; Menzer, S.; Nouwen, J.; Raymo, F. M.; Stoddart, J. F.; Williams, D. J. *J. Org. Chem.* **1996**, *61*, 9591–9595.

(20) Barnes, J. C.; Juríček, M.; Vermeulen, N. A.; Dale, E. J.; Stoddart, J. F. *J. Org. Chem.* **2013**, *78*, 11962–11969.

(21) (a) Liu, Z.; Nalluri, S. K. M.; Stoddart, J. F. *Chem. Soc. Rev.* **2017**, *46*, 2459–2478. (b) Cram, D. J.; Cram, J. M. *Container Molecules and Their Guests*; Royal Society of Chemistry: Cambridge, U.K., **1997**.

(22) (a) Bruns, C. J.; Stoddart, J. F. *The Nature of the Mechanical Bond: From Molecules to Machines*; John Wiley & Sons: Hoboken, NJ, **2017**. (b) Barnes, J. C.; Fahrenbach, A. C.; Cao, D.; Dyar, S. M.; Frasconi, M.; Giesener, M. A.; Benítez, D.; Tkatchouk, E.; Chernyashevskyy, O.; Shin, W. H.; Li, H.; Sampath, S.; Stern, C. L.; Sarjeant, A. A.; Hartlieb, K. J.; Liu, Z.; Carmieli, R.; Botros, Y. Y.; Choi, J. W.; Slawin, A. M. Z.; Ketterson, J. B.; Wasielewski, M. R.; Goddard, W. A., III; Stoddart, J. F. *Science* **2013**, *339*, 429–433. (c) Lipke, M. C.; Wu, Y.; Roy, I.; Wang, Y.; Wasielewski, M. R.; Stoddart, J. F. **2018**, *4*, 362–371.

(23) Barnes, J. C.; Juríček, M.; Strutt, N. L.; Frasconi, M.; Sampath, S.; Giesener, M. A.; McGrier, P. L.; Bruns, C. J.; Stern, C. L.; Sarjeant, A. A.; Stoddart, J. F. *J. Am. Chem. Soc.* **2013**, *135*, 183–192.

(24) Juríček, M.; Strutt, N. L.; Barnes, J. C.; Butterfield, A. M.; Dale, E. J.; Baldridge, K. K.; Stoddart, J. F.; Siegel, J. S. *Nat. Chem.* **2014**, *6*, 222–228.

(25) Gong, X.; Young, R. M.; Hartlieb, K. J.; Miller, C.; Wu, Y.; Xiao, H.; Li, P.; Hafezi, N.; Zhou, J.; Ma, L.; Cheng, T.; Goddard, W. A., III; Farha, O. K.; Hupp, J. T.; Wasielewski, M. R.; Stoddart, J. F. *J. Am. Chem. Soc.* **2017**, *139*, 4107–4116. (b) Dyar, S. M.; Barnes, J. C.; Juríček, M.; Stoddart, J. F.; Co, D. T.; Young, R. M.; Wasielewski, M. R. *Angew. Chem. Int. Ed.* **2014**, *53*, 5371–5375. (c) Young, R. M.; Dyar, S. M.; Barnes, J. C.; Juríček, M.; Stoddart, J. F.; Co, D. T.; Wasielewski, M. R. *J. Phys. Chem. A* **2013**, *117*, 12438–12448. (d) Dyar, S. M.; Barnes, J. C.; Juríček, M., Stoddart, J. F.; Co, D. T.; Young, R. M.; Wasielewski, M. R. *Angew. Chem. Int. Ed.* **2014**, *126*, 5475–5479.

(26) Coskun, A.; Spruell, J. M.; Barin, G.; Dichtel, W. R.; Flood, A. H.; Botros, Y. Y.;

Stoddart, J. F. *Chem. Soc. Rev.* **2012**, *41*, 4827–4859.

(27) Stoddart, J. F. *Angew. Chem. Int. Ed.* **2017**, *56*, 11094–11125.

(28) Wang, Y.; Sun, J.; Liu, Z.; Nassar, M. S.; Botros, Y. Y.; Stoddart, J. F. *Chem. Sci.* **2017**, *8*, 2562–2568.

(29) Xie, J.; Lee, S.; Chen, X. *Adv. Drug Deliv. Rev.* **2010**, *62*, 1064–1079.

(30) (a) Suseela, Y. V.; Das, S.; Pati, S. K.; Govindaraju, T. *ChemBioChem* **2016**, *17*, 2162 – 2171. (b) Yen, S. F.; Gabbay, E. J.; Wilson, W. D. *Biochemistry* **1982**, *21*, 2070−2076.

(31) Hisamatsu, S.; Masu, H.; Azumaya, I.; Takahashi, M.; Kishikawa, K.; Kohmoto, S. *Cryst. Growth Des.* **2011**, *11*, 5387–5395.

(32) Wu, Y.; Zhou, J.; Phelan, B. T.; Mauck, C. M.; Stoddart, J.F.; Young, R. M.; Wasielewski, M. R. *J. Am. Chem. Soc.*, **2017**, *139*, 14265–14276

(33) Hartlieb, K. J.; Witus, L. S.; Ferris, D. P.; Basuray, A. N.; Algaradah, M. M.; Sarjeant, A. A.; Stern, C. L.; Nassar, M. S.; Botros, Y. Y.; Stoddart, J. F. *ACS Nano* **2015**, *9*, 1461–1470.

(34) I. Haq, Reversible small molecule-nucleic acid interactions, in *Nucleic Acids in Chemistry and Biology*, ed. Blackburn, G. M.; Gait, M. J.; Loakes D.; Williams, D. M. The Royal Society of Chemistry, Cambridge, **2006**, pp. 341–382

(35) (a) Liu, Z.; Zhao, H.; Liu, W.; Li, T.; Wang, Y.; Zhao, M. *Inflammation* **2014**, *38*, 433–444. (b) Tong, C.; Xiang, G.; Bai, Y. *J. Agric. Food Chem.* **2010**, *58*, 5257–5262. (b) Hendry, L. B.; Mahesh, V. B.; Bransome, E. D.; Ewing, D. E. *Mutat. Res.* **2007**, *623*, 53–71.

Captions of Schemes and Figures

Scheme 1. Synthesis of **6**•4X (**6**•4X, X = PF_6^-, Cl^-).

Figure 1. Solid-state (super)structures of the $\mathbf{6}^{4+}$ obtained from single-crystal X-ray crystallography. (a) A stick representation showing the distances and the torsional angles associated with the box-like geometry. (b-c) Stick representations of different side views of the $\mathbf{6}^{4+}$. (d) Space-filling representation of a $\mathbf{6}^{4+}$ superstructure showing that the $\mathbf{ExBIPY}^{2+}$ and $\mathbf{TzBIPY}^{2+}$ units are facing each other. (e) Solid-state superstructure of $\mathbf{6}^{4+}$ revealing a zigzag arrangement.

Figure 2. (a) Absorption (red) and emission (blue) spectra of **6**•4Cl in H_2O (Inset: fluorescence lifetime decay). (b) fsTA spectra of **6**•4Cl in H_2O, 414 nm excitation. (d) Cyclic voltammogram and DPV of $\mathbf{6}^{4+}$.

Figure 3. Effect of different concentrations of **6**•4Cl, **4**•2Cl and **2**•2Cl on RAW 264.7 cells viability after 24 h incubation. The cell viability was assessed using the MTT assay. The values presented are the mean ± SD (n=3).

Figure 4. Live-cell confocal microscopy images of RAW 264.7 macrophages cells. Cells were incubated with (a) SYTO nuclei, (b) **6**•4Cl (20 μM in PBS solution). (c-d) Composed images of the cells with red and blue channel. Cells were incubated with (e) LysoTracker green, (f) **6**•4Cl (20 μM in PBS solution), (g) Composed images of the cells with green and blue channel, (h) zoom-in section of **g** showing the co-compartmentalization of **6**•4Cl and LysoTracker green showing the presence of **6**•4Cl into the lysosome of the living cells. Z-stacks of images were deconvolved using ImageJ package. Scale bar, 10 μm.

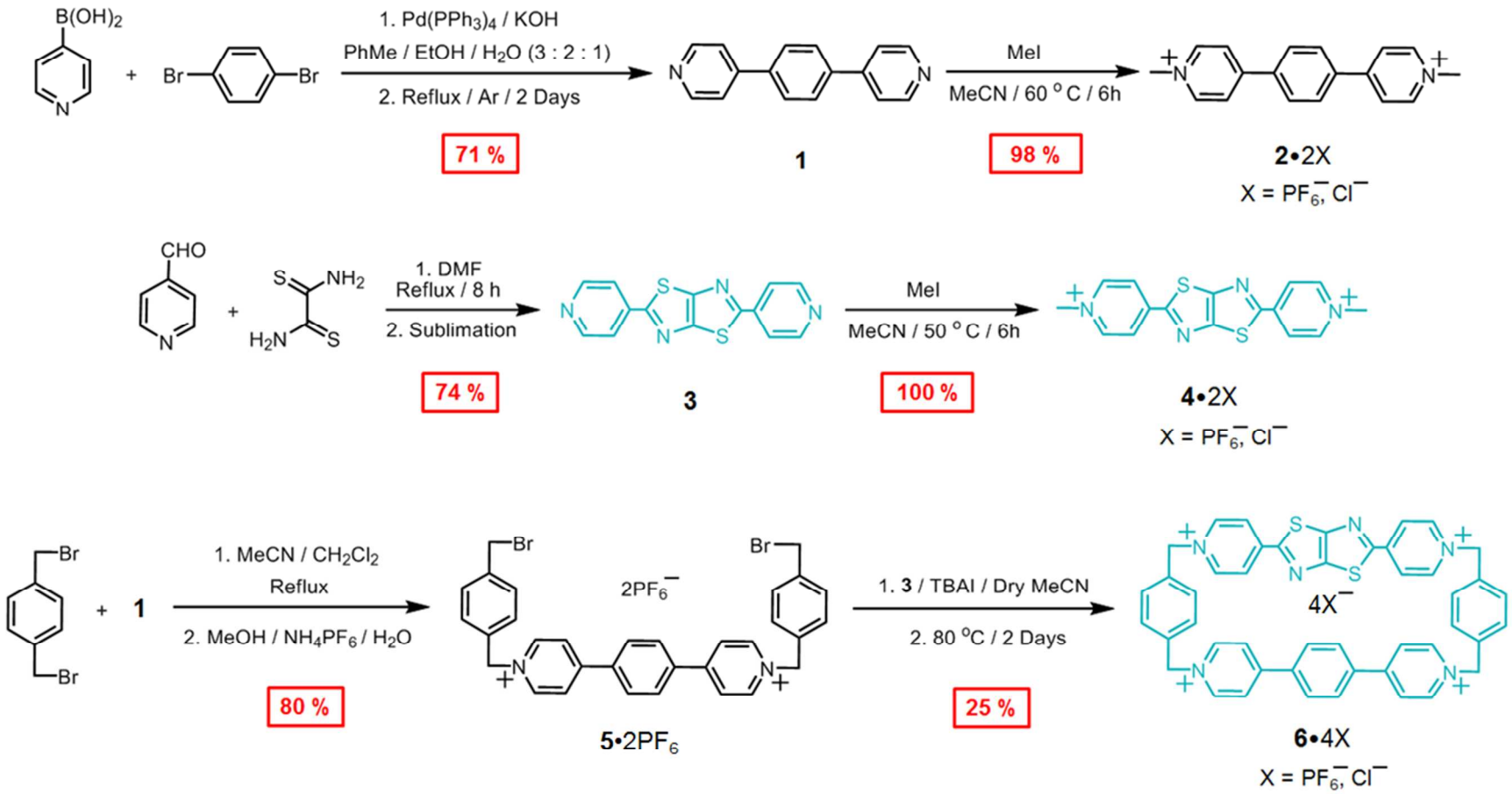
B(OH)2
Br
Br
1. Pd(PPh3)4 / KOH
PhMe / EtOH / H2O (3 : 2 : 1)
2. Reflux / Ar / 2 Days
71 %
1
MeI
MeCN / 60 °C / 6h
98 %
2•2X
X = PF6−, Cl−
CHO
NH2
H2N
S
1. DMF
Reflux / 8 h
2. Sublimation
74 %
3
MeI
MeCN / 50 °C / 6h
100 %
4•2X
X = PF6−, Cl−
Br
Br
1
1. MeCN / CH2Cl2
Reflux
2. MeOH / NH4PF6 / H2O
80 %
2PF6−
5•2PF6
1. 3 / TBAI / Dry MeCN
2. 80 °C / 2 Days
25 %
4X−
6•4X
X = PF6−, Cl−

Scheme 1

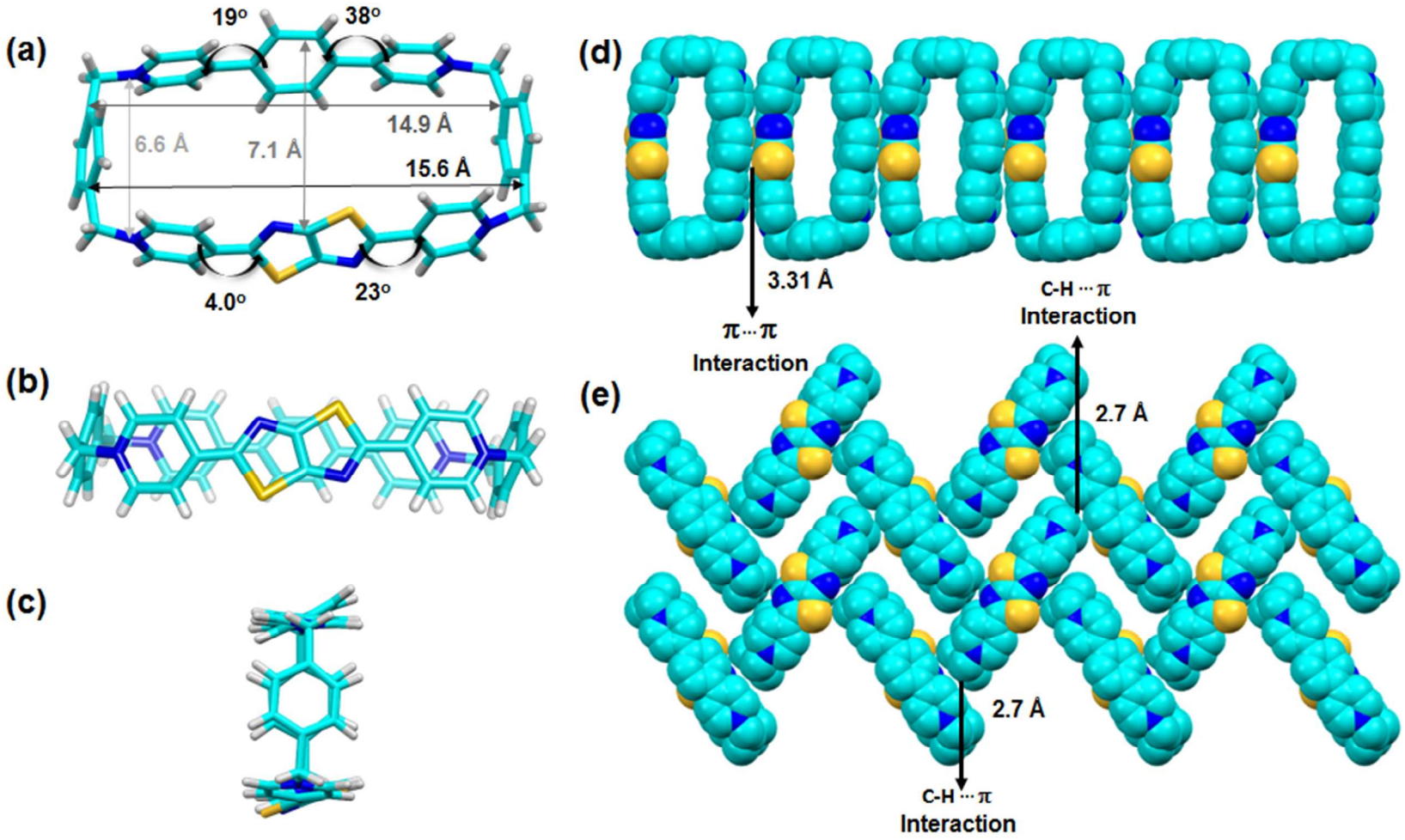
(a)
19°
38°
14.9 Å
6.6 Å
7.1 Å
15.6 Å
4.0°
23°
(b)
(c)
(d)
3.31 Å
π···π
Interaction
C-H ··· π
Interaction
(e)
2.7 Å
2.7 Å
C-H ··· π
Interaction

Figure 1

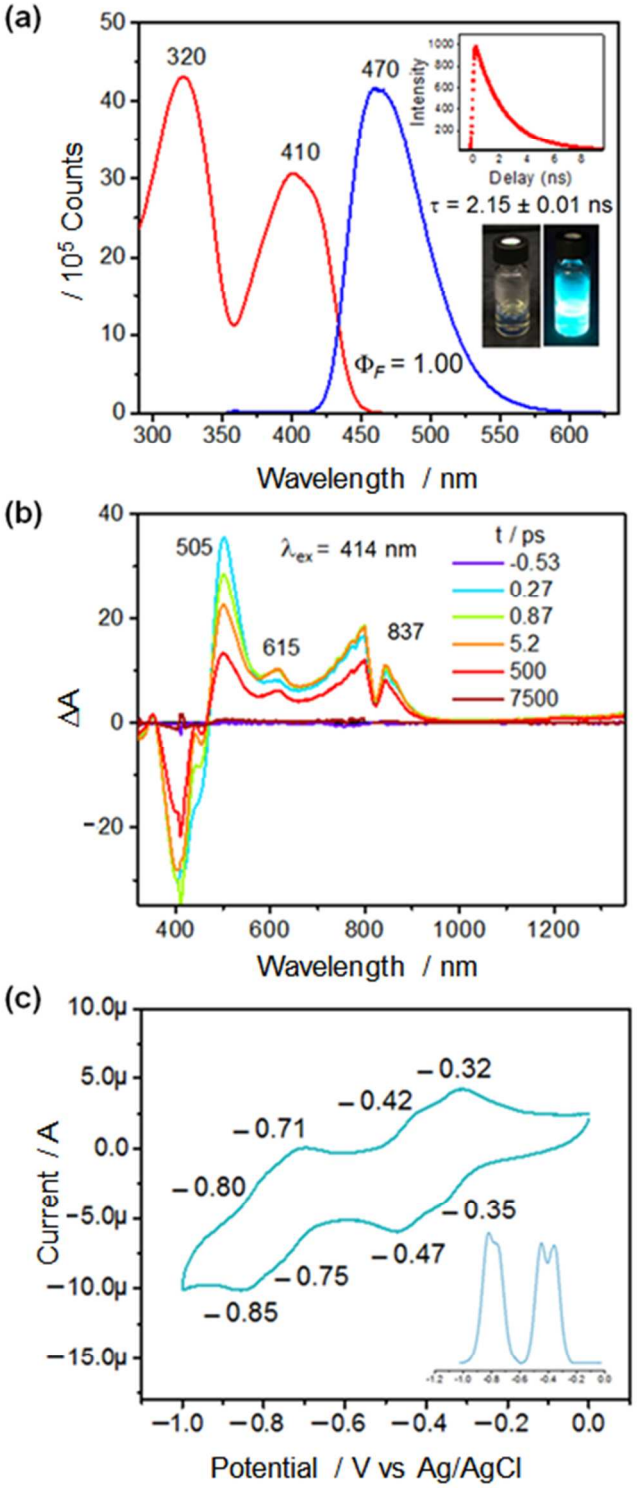
(a)
320
410
470
/ 10^5 Counts
Wavelength / nm
Intensity
Delay (ns)
τ = 2.15 ± 0.01 ns
Φ_F = 1.00
(b)
505
615
837
λ_ex = 414 nm
t / ps
-0.53
0.27
0.87
5.2
500
7500
ΔA
Wavelength / nm
(c)
−0.32
−0.42
−0.71
−0.80
−0.35
−0.47
−0.75
−0.85
Current / A
Potential / V vs Ag/AgCl

Figure 2

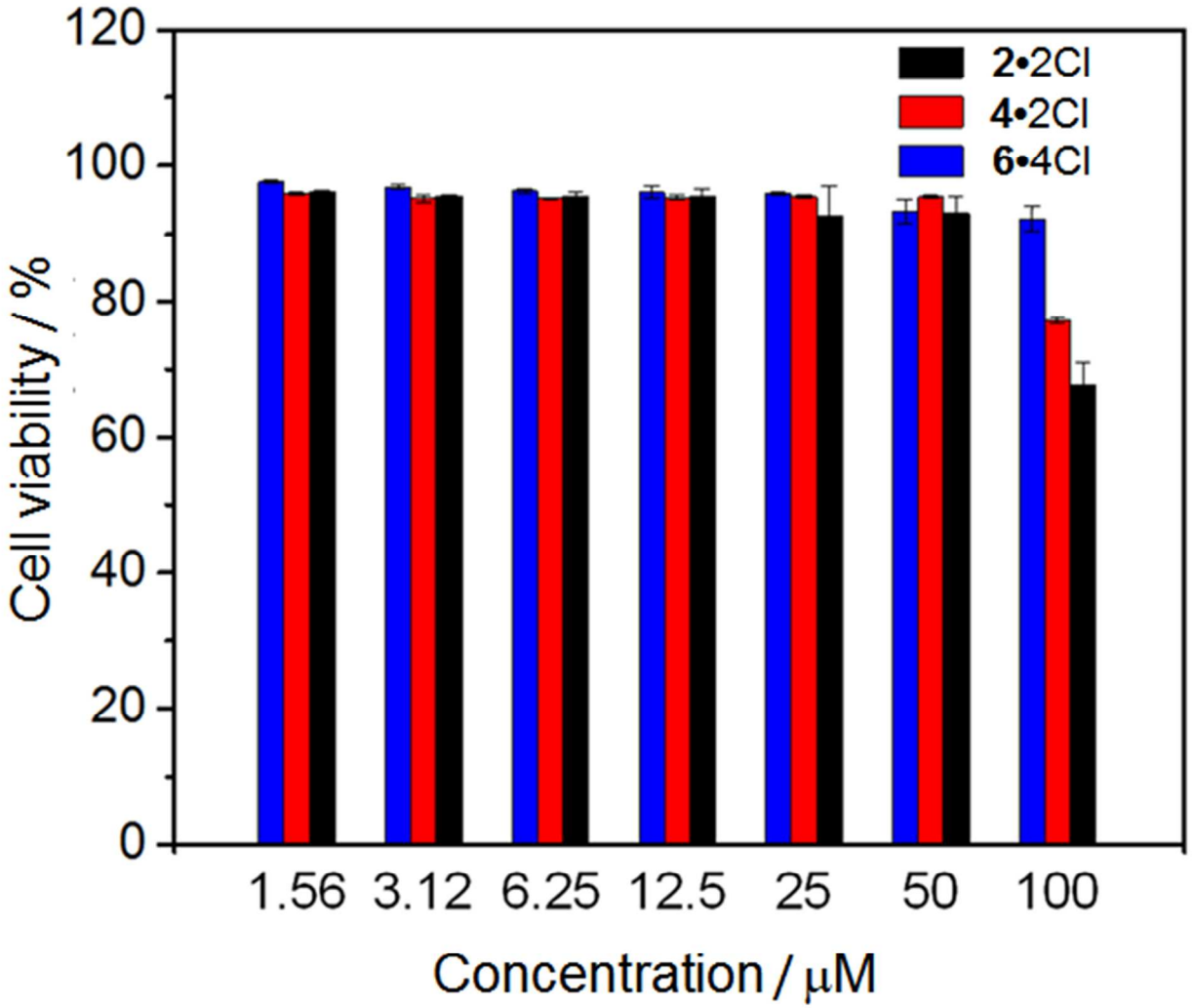
120
100
80
60
40
20
0
Cell viability / %
2•2Cl
4•2Cl
6•4Cl
1.56
3.12
6.25
12.5
25
50
100
Concentration / μM

Figure 3

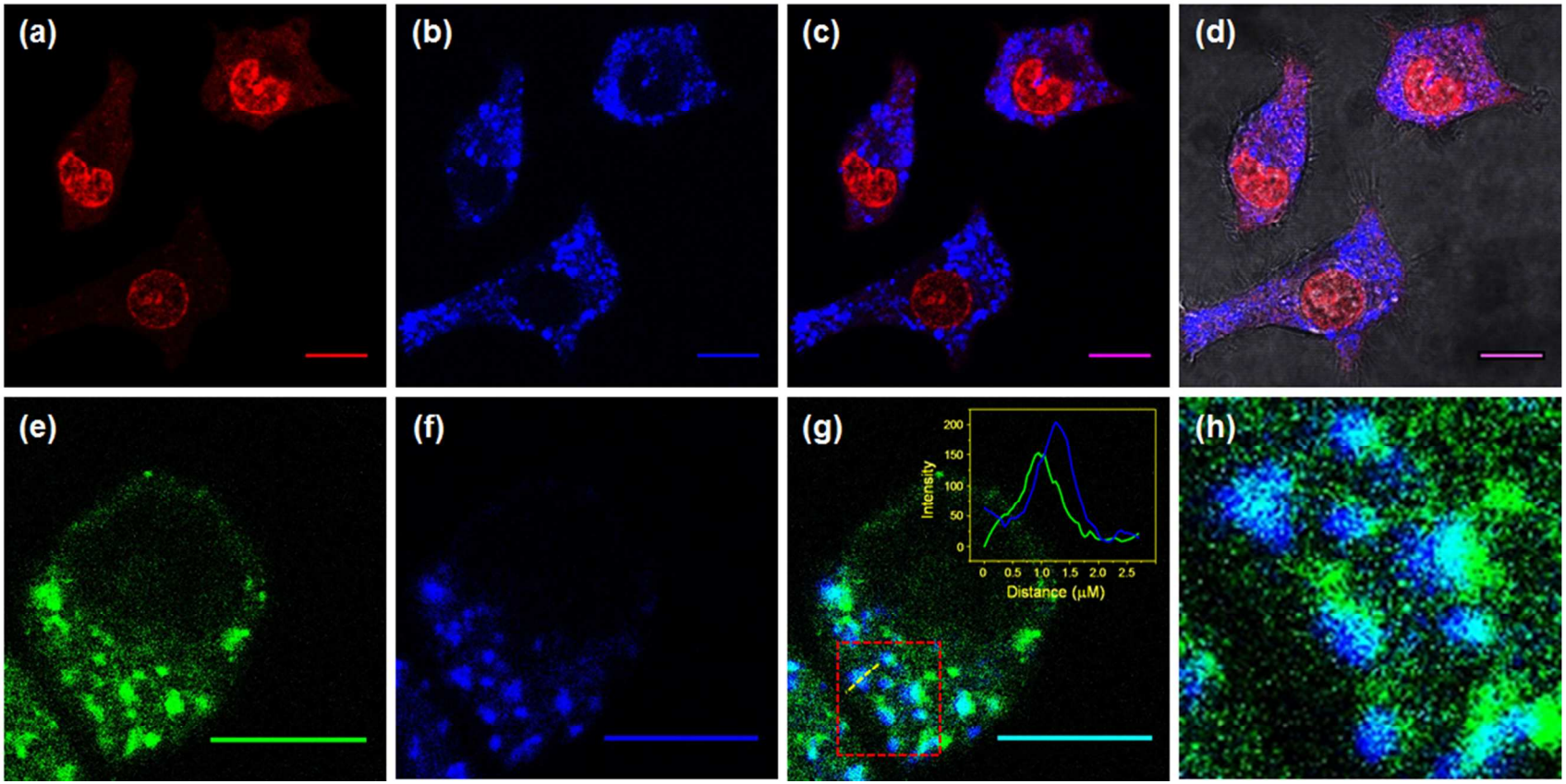
(a)
(b)
(c)
(d)
(e)
(f)
(g)
(h)
Intensity
200
150
100
50
0
0 0.5 1.0 1.5 2.0 2.5
Distance (μM)

Figure 4

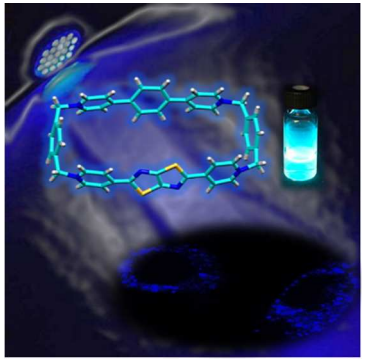

TOC graphic